

1 **Expansions of adaptive-like NK cells with a tissue-resident**
2 **phenotype in human lung and blood**

3

4 Nicole Marquardt^{1*}, Marlena Scharenberg¹, Jeffrey E. Mold², Joanna Hård², Eliisa
5 Kekäläinen^{3,4}, Marcus Buggert¹, Son Nguyen^{5,6}, Jennifer N. Wilson¹, Mamdoh Al-
6 Ameri⁷, Hans-Gustaf Ljunggren¹, Jakob Michaëlsson¹

7

8 Running title: Adaptive-like human lung tissue-resident NK cells

9

10 **Affiliations:**

11 ¹Center for Infectious Medicine, Department of Medicine, Karolinska Institutet,
12 Stockholm, Sweden

13 ²Department of Cell and Molecular Biology, Karolinska Institutet, Stockholm, Sweden

14 ³Translational Immunology Research Program & Department of Bacteriology and
15 Immunology, University of Helsinki, Finland

16 ⁴HUSLAB, Division of Clinical Microbiology, Helsinki University Hospital, Helsinki,
17 Finland,

18 ⁵Department of Microbiology, Perelman School of Medicine, University of
19 Pennsylvania, Philadelphia, PA, USA

20 ⁶Institute for Immunology, Perelman School of Medicine, University of Pennsylvania,
21 Philadelphia, PA, USA

22 ⁷Thoracic Surgery, Department of Molecular Medicine and Surgery, Karolinska
23 Institutet, Karolinska University Hospital, Stockholm, Sweden

24

25

26 ***Corresponding author/Lead contact:** Nicole Marquardt, Center for Infectious
27 Medicine, Department of Medicine, Karolinska Institutet, 141 52 Huddinge, Sweden;
28 E-mail: nicole.marquardt@ki.se, Phone: +46-8-58589791 Fax: +468-7467637.
29 ORCID: <https://orcid.org/0000-0003-3186-4752>

30 **Abstract**

31 Human adaptive-like "memory" CD56^{dim}CD16⁺ NK cells in peripheral blood from
32 cytomegalovirus-seropositive individuals have been extensively investigated in recent
33 years and are currently explored as a treatment strategy for hematological cancers.
34 However, treatment of solid tumors remains limited due to insufficient NK cell tumor
35 infiltration, and it is unknown whether large expansions of adaptive-like NK cells that
36 are equipped for tissue-residency and tumor-homing exist in peripheral tissues. Here,
37 we show that human lung and blood contains adaptive-like CD56^{bright}CD16⁻ NK cells
38 with hallmarks of tissue-residency, including expression of CD49a. Expansions of
39 adaptive-like lung tissue-resident (tr)NK cells were found to be present independently
40 of adaptive-like CD56^{dim}CD16⁺ NK cells and to be hyperresponsive towards target
41 cells. Together, our data demonstrate that phenotypically, functionally, and
42 developmentally distinct subsets of adaptive-like NK cells exist in human lung and
43 blood. Given their tissue-related character and hyperresponsiveness, human lung
44 adaptive-like trNK cells might represent a suitable alternative for therapies targeting
45 solid tumors.

46 **Key words:** NK cells, adaptive, memory, lung, tissue-resident

47

48 **Abbreviations:**

49 Eomes: Eomesodermin

50 FITC: Fluorescein isothiocyanate

51 HCMV: Human cytomegalovirus

52 ILC: Innate lymphoid cell

53 KIR: Killer cell immunoglobulin-like receptor

54 NK: Natural killer

55 PE: Phycoerythrin

56 ROS: Reactive oxygen species

57 **Introduction**

58 Natural killer (NK) cells are a crucial component of the innate immune system. They
59 target and eliminate virus-infected and malignant cells, and boost immunity through the
60 production of proinflammatory cytokines including IFN- γ and TNF. In recent years,
61 the concept of adaptive-like or “memory” NK cells has emerged from studies in mice
62 (1-4) and humans (5-10). These adaptive-like NK cells share a distinct phenotype and
63 increased target cell responsiveness as well as having features of longevity and superior
64 recall potential reminiscent of memory T cells (11).

65 Most studies of human adaptive-like NK cells have focused on subsets of
66 NKG2C⁺(KIR⁺)CD56^{dim}CD16⁺ NK cells, originally found to be expanded and stably
67 imprinted in peripheral blood of approximately 30-40% of human CMV (HCMV)
68 seropositive individuals (5,10). Adaptive-like NKG2C⁺(KIR⁺)CD56^{dim}CD16⁺ NK cells
69 in human peripheral blood have a distinctive phenotypic (5,10), epigenetic (8,9), and
70 functional (8-10) profile compared to conventional NK cells and have been suggested
71 to contribute to immunity against HCMV (1,12). Importantly, adaptive-like peripheral
72 blood-derived CD56^{dim}CD16⁺ NK cells (herein defined as adaptive-like
73 CD56^{dim}CD16⁺ pbNK cells) are currently explored for improving NK cell-mediated
74 cancer therapies. While adoptive NK cell transfer showed optimistic results in the
75 treatment of hematological malignancies (reviewed in (13)), targeting solid tumors was
76 less successful due to poor migration to and infiltration into the tumor (reviewed in
77 (13)). In these cases, adaptive-like NK cells with an increased capacity to infiltrate
78 tissues e.g. through co-expression of tissue-specific ligands might be desirable. In fact,
79 similar approaches for targeting solid tumors have recently been suggested for T_{RM} cells
80 (14).

81 We and others recently identified a subset of tissue-resident
82 CD49a⁺CD56^{bright}CD16⁻ NK (trNK) cells in the human lung (15,16). The human lung

83 is a frequent site of acute infections, including infections with viruses such as influenza
84 virus, respiratory syncytial virus (RSV), and HCMV, as well as serving as a reservoir
85 for latent HCMV infection (17). Although human CD56^{dim}CD16⁺ lung NK cells are
86 hyporesponsive to *ex vivo* target cell stimulation (18), exposure of human lung NK cells
87 to virus-infected cells is likely to result in functional NK cell priming and expansion of
88 distinct NK cell subsets. Indeed, increased polyfunctional responses have been
89 observed in CD16⁻ lung NK cells following *in vitro* infection with IAV (16,19).
90 However, the presence of expansions of functional adaptive-like trNK cells in the
91 human lung is to date unknown.

92 Here, we identify and examine a CD49a⁺KIR⁺NKG2C⁺CD56^{bright}CD16⁻ NK
93 cell population with features of tissue-resident NK cells in human lung and blood,
94 which is distinct from adaptive-like CD56^{dim}CD16⁺ pbNK cells. In donors with
95 expansions of adaptive-like CD49a⁺ lung trNK cells, small but detectable frequencies
96 of adaptive-like CD49a⁺ NK cells were observed in paired peripheral blood. While
97 adaptive-like CD56^{dim}CD16⁺ pbNK cells (as commonly identified in peripheral blood
98 of HCMV-seropositive donors) and adaptive-like CD49a⁺ trNK cells in lung and blood
99 shared a common core gene signature, we identified several unique features of each
100 population indicating that they may represent developmentally distinct populations.
101 Notably, NK cells from donors with an adaptive-like trNK cell expansion in the lung
102 were hyperresponsive towards target cells. Thus, we provide evidence indicating that
103 CD49a⁺KIR⁺NKG2C⁺CD56^{bright}CD16⁻ trNK cells in the human lung represent a
104 distinct population of adaptive-like NK cells with potential implications in lung
105 surveillance and future treatment options of solid tumors.

106 **Results**

107 *Adaptive-like NK cells can be identified in human lung*

108 We first set out to investigate whether expansions of adaptive-like
109 KIR⁺NKG2C⁺ NK cells could be identified in the human lung. The majority of NK
110 cells in the lung are phenotypically similar to pbNK cells (CD69⁻CD56^{dim}CD16⁺),
111 suggesting that these cells may recirculate between the lungs and peripheral blood (18).
112 Accordingly, circulating populations of expanded adaptive-like CD56^{dim}CD16⁺ NK
113 cells could also be identified in both the peripheral blood and lungs from patients
114 undergoing surgery for suspected lung cancer (Fig. 1A). Surprisingly, KIR and NKG2C
115 were also co-expressed on less differentiated CD56^{bright}CD16⁻ lung NK cells in many
116 of the patients included in the study, with varying frequencies between donors (Fig. 1B,
117 C) (see Supplementary Fig. 1A for the gating strategy to identify KIR⁺NKG2C⁺
118 CD56^{bright}CD16⁻ and CD56^{dim}CD16⁺ NK cells). In several donors the frequencies of
119 KIR⁺NKG2C⁺CD56^{bright}CD16⁻ NK cells in human lung vastly exceeded those
120 previously described for CD16⁻ NK cells in the liver (7), with up to 98% of
121 CD56^{bright}CD16⁻ lung NK cells co-expressing KIR and NKG2C (Fig. 1 A, B).

122 Next, we assessed phenotypic features of KIR⁺NKG2C⁺CD56^{bright}CD16⁻ lung
123 NK cells in an unbiased manner using high dimensional flow cytometry. Uniform
124 manifold approximation and expression (UMAP) analysis revealed a distinct subset of
125 cells with an expression pattern consistent with adaptive-like NK cells found in
126 peripheral blood and liver, including low expression of Siglec-7 and CD161, and high
127 expression of NKG2C, KIRs, and CD2 (7,8,20,21) (Fig. 1D). Unlike adaptive-like
128 CD56^{dim}CD16⁺ pbNK cells, KIR⁺NKG2C⁺CD56^{bright}CD16⁻ NK cells expressed lower
129 levels of CD45RA and NKp80, and higher levels of CD8 (Fig. 1D). In addition, to these
130 expression patterns, manual analysis of individual samples additionally confirmed low
131 expression of ILT2 and FcεR1γ, as compared to KIR⁺NKG2C⁺CD56^{dim}CD16⁺ lung NK

132 cells (Fig. 1E, F). Furthermore, $KIR^+NKG2C^+CD56^{bright}CD16^-$ lung NK cells displayed
133 low expression of $ILT2$ and $Fc\epsilon R1\gamma$ and high expression of $Eomes$ and $NKG2A$, but
134 similar levels in $T-bet$ expression, revealing a phenotype distinct from human adaptive-
135 like $KIR^+NKG2C^+CD16^-$ NK cells in the liver (7) (Fig. 1E, F). Together, our data reveal
136 the presence of a previously uncharacterized population of an adaptive-like NK cell
137 subset, herein identified as $KIR^+NKG2C^+CD56^{bright}CD16^-$, in the human lung, which
138 is distinct from adaptive-like $CD56^{dim}CD16^+$ pbNK cells.

139

140 *Adaptive-like $CD56^{bright}CD16^-$ NK cells in human lung are tissue-resident*

141 TrNK cells in human lung are characterized by expression of $CD69$ and the
142 integrins $CD49a$ and $CD103$ (15,16), while adaptive-like NK cells have not yet been
143 described within this subset. Strikingly, the vast majority of the distinct population of
144 $NKG2C^+CD56^{bright}CD16^-$ NK cells identified by UMAP analysis co-expressed $CD69$
145 (80%) and $CD49a$ (77%), and a substantial proportion (38%) also co-expressed $CD103$
146 (Fig. 2A, B), suggesting tissue-residency of adaptive-like $CD56^{bright}CD16^-$ NK cells in
147 the lung. KIR^+NKG2C^+ NK cells co-expressing $CD49a$, $CD69$, or $CD103$, were mainly
148 $CD56^{bright}CD16^-$ (Fig. 2C, D), further demonstrating that they are clearly distinct from
149 adaptive-like $CD56^{dim}CD16^+$ pbNK cells.

150 To further characterize adaptive-like trNK cells in the lung, we compared the
151 gene expression profiles of sorted adaptive KIR^+NKG2C^+ and non-adaptive KIR^-
152 $NKG2C^-$ trNK cells in human lung using RNA sequencing (Fig. 2E, F; see sorting
153 strategy in Supplementary figure 1B, C). 102 genes were differentially expressed
154 ($p < 0.05$, $\log_2FC > 1$), including several KIR genes, $CD8A$, $GPR183$ ($EBI2$), $IRF8$ and
155 $SH2D1B$ ($EAT2$), and genes encoding for the transcription factors $MafF$ ($MAFF$) and
156 $ZNF498$ ($ZSCAN25$). $GPR183$ has been demonstrated to be crucial for tissue-specific
157 migration of innate lymphoid cells (22), while $EAT2$ expression has previously been

158 shown to be downregulated in adaptive-like CD56^{dim}CD16⁺ pbNK cells (8).
159 Interestingly, while upregulation of both *IRF8* and *THEMIS2* has been reported to be
160 essential for NK cell-mediated responses against MCMV infection (23,24), gene
161 expression of both molecules was low in adaptive-like trNK cells in human lung (Fig.
162 2E), indicating different activation pathways in adaptive-like NK cells in mice and
163 humans. Furthermore, we compared differentially expressed genes in adaptive-like
164 lung trNK cells *versus* CD56^{dim}CD16⁺ pbNK cells and observed an overlap of
165 approximately one third of the differentially expressed genes (GSE117614) (25). These
166 genes included *KLRC2* (NKG2C), *KLRC3* (NKG2E), *IL5RA*, *GZMH*, *ITGAD* (CD11d),
167 *RGS9*, *RGS10* (upregulated), and *KLRB1* (CD161), *KLRC1* (NKG2A), *KLRF1*
168 (NKp80), *TMIGD2*, *IL18RAP*, *FCER1G*, *MLC1*, *CLIC3* and *TLE1* (downregulated)
169 (Fig. 2F). These results demonstrate that adaptive-like lung trNK and CD56^{dim}CD16⁺
170 pbNK cells share a common core gene set specific for adaptive-like NK cells.

171 Adaptive-like NK cells in peripheral blood and in the human liver commonly
172 have a distinct KIR expression profile which is dominated by KIRs that bind to self-
173 HLA class I (self-KIRs) (7,10,26). In the lung, analysis of single KIR expression on
174 CD16⁻ and CD16⁺ NK cell subsets in donors with high frequencies of adaptive-like
175 lung trNK cells revealed that the former subset displayed unique KIR expression
176 patterns compared to CD16⁺ NK cells in paired blood or lung (Fig. 2G-I;
177 Supplementary Fig. 1D for the gating strategy). High expression of KIRs on the
178 adaptive-like trNK cells was limited to self-KIR, identical to the phenotype described
179 for adaptive-like NK cells in liver and peripheral blood. Notably, even in a donor with
180 adaptive-like NK cell expansions of both trNK cells and pbNK cells (Fig. 2G), the KIR-
181 expression profile differed between the two subsets. These results suggest a subset-
182 specific development and/or differentiation of adaptive-like NK cells in blood and lung.

183 Together, CD49a⁺KIR⁺NKG2C⁺CD56^{bright}CD16⁻ trNK cells in the human lung
184 exhibit a unique profile of activating and inhibitory NK cell receptors (e.g. NKG2A,
185 KIR, NKp80), as well as adaptor, signaling, and effector molecules (FcεR1γ, SH2D1B,
186 granzyme H). This indicates that these are bona fide adaptive-like trNK cells which are
187 distinct from adaptive-like CD56^{dim}CD16⁺ pbNK cells, demonstrating the presence of
188 an as of yet unexplored NK cell population in the human lung.

189

190 *Lung adaptive-like trNK cells are hyperresponsive to target cells*

191 In order to determine whether adaptive-like lung trNK cells differed
192 functionally from non-adaptive CD56^{bright}CD16⁻ lung trNK cells, we first compared
193 expression levels of genes associated with functional competence (Fig. 3A). Gene
194 expression in adaptive-like lung trNK cells was higher for *IFNG*, *IL32*, *XCL1* and
195 *GZMH* (granzyme H), and lower for *GZMA* (granzyme A), *GZMK*
196 (granzyme K), *IL2RB* (CD122) and *IL18RAP* as compared to non-adaptive lung trNK
197 cells (Fig. 3A). These results suggest a potential cytokine-mediated priming of
198 adaptive-like trNK cells *in vivo*, e.g. by IL-12 and IL-18, which are potent inducers of
199 IFN-γ and IL-32 in NK cells (27). While expression levels of the effector molecules
200 *PRF1* (perforin) and *GZMB* (granzyme B) did not differ between adaptive- and non-
201 adaptive-like CD56^{bright}CD16⁻ NK cells at transcriptome level (Fig. 3A), *ex vivo* protein
202 expression was increased for granzyme B in adaptive-like trNK cells (Fig. 3B, C). This
203 indicated a potential cytotoxic function in this particular subset, despite lung NK cells
204 generally being characterized as hyporesponsive to target cell stimulation (16,18).
205 Intriguingly, NK cells from donors with an expansion of adaptive-like trNK cells in the
206 lung degranulated stronger and produced more TNF compared to those from donors
207 without such expansions (Fig. 3D). In particular NK cells co-expressing CD49a and
208 KIR degranulated strongly and produced high levels of TNF upon target cell

209 stimulation (Fig. 3D-F). This hyperresponsiveness of adaptive-like lung trNK cells was
210 independent from co-expression of CD103, since similar activation levels were
211 observed between CD49a⁺CD103⁻ and CD49a⁺CD103⁺ KIR⁺NKG2C⁺ NK cells (Fig.
212 3F-H). Furthermore, blood NK cells from donors with expanded adaptive-like lung
213 trNK cells also responded stronger to target cells as compared to donors without such
214 expansions (Fig. 3F-H). Taken together, these results revealed that the presence of
215 expanded adaptive-like trNK cells in the lung is linked to hyperresponsivity towards
216 target cells, implicating a role of these cells in active immune regulation within the
217 lung.

218

219 *Adaptive-like CD49a⁺CD56^{bright}CD16⁻ NK cells can be identified in matched patient*
220 *peripheral blood*

221 As a hallmark of tissue-resident cells, CD49a is commonly expressed on subsets of T
222 cells and NK cells in non-lymphoid compartments such as the lung (15,16,19,28), liver
223 (7), skin (29), uterus (30), and intestine (31), but not in peripheral blood. Intriguingly,
224 however, we identified a small subset of CD49a⁺KIR⁺NKG2C⁺ NK cells within the
225 CD16⁻ NK cell population in paired peripheral blood of donors harboring expansions
226 of adaptive-like trNK cells in the lung (Fig. 4A, B, see gating strategy in Supplementary
227 Fig. 1E). The frequencies of CD49a⁺KIR⁺NKG2C⁺CD16⁻ NK cells in peripheral blood
228 (herein identified as CD49a⁺ pbNK cells) were overall considerably lower as compared
229 to either adaptive-like lung trNK cells or CD56^{dim}CD16⁺ pbNK cells, respectively (Fig.
230 4B). We observed that 18.6% and 25.6% of all donors had an expansion (identified as
231 outliers) of adaptive-like CD49a⁺CD56^{bright}CD16⁻ NK cells in lung and paired
232 peripheral blood, respectively. In comparison, 20.9% and 15.1% of all donors had an
233 expansion of adaptive-like CD56^{dim}CD16⁺ pbNK cells in lung and paired blood,
234 respectively (Fig. 4B). Interestingly, expansions of adaptive-like

235 CD49a⁺CD56^{bright}CD16⁻ NK and CD56^{dim}CD16⁺ pbNK cells were virtually mutually
236 exclusive in donors (Fig. 4C). However, there was a substantial overlap within each of
237 these subsets between lung and peripheral blood (Fig. 4C), that is, e.g. a high likelihood
238 of having an expansion of adaptive-like trNK cells in the lung if an expansion of
239 adaptive-like CD49a⁺ NK cells was present in the paired blood, and *vice versa*. This
240 distinct distribution of adaptive-like NK cell populations per donor suggests adaptive-
241 like CD49a⁺CD56^{bright}CD16⁻ and CD56^{dim}CD16⁻ pbNK cells are developing
242 independently from each other. We next analyzed the phenotype of adaptive-like
243 CD49a⁺CD56^{bright}CD16⁻ pbNK cells and found intermediate expression of CD57 with
244 relatively low co-expression of NKG2A (Fig. 4D, E), in contrast to lower expression
245 of CD57 and higher expression of NKG2A in the adaptive-like lung trNK cells (Fig.
246 1E, F). Furthermore, adaptive-like CD49a⁺CD56^{bright}CD16⁻ pbNK cells differed from
247 their counterpart in lung by low expression of both CD69 and CD103 (Fig. 4E, D),
248 consistent with known phenotypic differences between tissue-resident and circulatory
249 lymphocyte populations (15,32-34).

250 Taken together, these results demonstrate the presence of an adaptive-like
251 CD49a⁺CD56^{bright}CD16⁻ NK cell subset in the peripheral blood of a subset of donors,
252 which is linked to adaptive-like trNK cells in the human lung and emerging
253 independently from CD56^{dim}CD16⁺ adaptive-like pbNK cells.

254

255 *Peripheral blood adaptive-like CD49a⁺CD56^{bright}CD16⁻ pbNK cells from healthy*
256 *donors share features with lung trNK cells and adaptive-like CD56^{dim}CD16⁺ pbNK*
257 *cells*

258 The presence of adaptive-like lung trNK cells in patients undergoing surgery for
259 suspected lung cancer did not significantly correlate with any demographical or clinical
260 parameters including age, gender, cigarette smoking, COPD, the type of lung tumor,

261 survival, lung function, or HCMV IgG concentrations in plasma (Supplementary Fig.
262 2A-F). Since we could identify circulating CD49a⁺CD56^{bright}CD16⁻ pbNK cells in the
263 majority of patients with an expansion of adaptive-like trNK cells in the lung, we next
264 sought to determine if such cells could also be detected in the peripheral blood of
265 unrelated healthy donors. Indeed, we found KIR⁺NKG2C⁺ NK cells co-expressing
266 CD49a in the CD56^{bright}CD16⁻ NK cell subset in 16% of healthy blood donors (Fig. 5A,
267 B). The frequencies of CD49a⁺CD56^{bright}CD16⁻ pbNK cells out of CD16⁻ NK cells were
268 lower in healthy peripheral blood (up to 5%, mean 0.3%) as compared to those found
269 in patients with suspected lung cancer (up to 21%, mean 1.2%) (Fig. 5B). Within the
270 CD56^{bright}CD16⁻ NK cell subset, KIR⁺NKG2C⁺ NK cells were almost exclusively
271 detected in the CD49a⁺ population (Fig. 5C). UMAP analysis of CD56^{bright}CD16⁻ NK
272 cells from healthy donors with CD49a⁺CD56^{bright}CD16⁻ NK cells in the blood revealed
273 a strong separation of the CD49a⁺ NK cell subset co-expressing KIR and NKG2C based
274 on lower expression or lack of CD69, CD45RA, CD57, CD38, NKp80, and TIM-3 as
275 well as high expression of CD8, CXCR3 and granzyme B on CD49a⁺KIR⁺NKG2C⁺
276 NK cells (Fig. 5D). This phenotype could be confirmed in individual samples (Fig. 5E).
277 Interestingly, strong expression of CXCR6 could be identified on CD69⁺, but not on
278 adaptive-like CD49a⁺ CD56^{bright}CD16⁻ pbNK cells, indicating that the latter NK cell
279 subset depends on other chemokine receptors such as CXCR3 for tissue homing.

280 To gain further insight into the adaptive-like CD49a⁺ pbNK cells, we sorted this
281 subset and compared it to sorted blood non-adaptive CD49a⁻CD56^{bright}CD16⁻ NK cells
282 using RNAseq (Fig. 6A, see Supplementary Fig. 1C for gating strategy). We next
283 investigated whether gene expression differences in adaptive-like CD49a⁺ pbNK cells
284 indicated a different functional profile. Adaptive-like CD49a⁺ pbNK cells expressed
285 particularly higher levels of *CCL5*, *LAMP1*, *GZMH* and *GNLY*, and lower levels of
286 *XCL1*, *HIF1A*, *IL2RB*, and *L18RAP* (Fig. 5F). Hence, adaptive-like CD49a⁺ pbNK cells

287 and adaptive-like lung trNK cells from different donors (Fig. 3A) shared a common
288 gene expression pattern for some (*CCL5*, *GZMH*, *IL2RB* and *IL18RAP*), but not all (i.e.,
289 *GNLY*) genes, indicating that they are functionally distinct from each other but also
290 from their non-adaptive counterparts.

291 To assess whether adaptive-like CD49a⁺CD56^{bright}CD16⁻ pbNK cells segregate
292 further at the transcriptome level, we analyzed differentially expressed genes between
293 adaptive-like CD49a⁺CD56^{bright}CD16⁻ pbNK cells and non-adaptive CD56^{bright}CD16⁻
294 NK cells in peripheral blood from healthy blood donors. A total of 351 genes were
295 differentially expressed ($\text{padj} < 0.01$, $\log_2\text{FC} > 1$) and clearly segregated both subsets
296 (Fig. 6A). Since adaptive-like CD49a⁺ pbNK cells resembled to some extent adaptive-
297 like trNK cells in the lung, we next sought to identify similarities to non-adaptive and
298 adaptive-like trNK cells also at transcriptome level. For this, we compared
299 differentially expressed genes in adaptive-like CD49a⁺CD56^{bright}CD16⁻ pbNK cells
300 (compared to CD49a⁻KIR⁻CD56^{bright}CD16⁻ NK cells in peripheral blood) and in non-
301 adaptive lung trNK cells (defined as CD69⁺CD49a⁺CD103⁺NKG2A⁺NKG2C⁻CD16⁻
302 NK cells) (compared to non-tissue-resident CD69⁻CD56^{bright}CD16⁻ NK cells in lung)
303 (Fig. 6B). Adaptive-like CD49a⁺CD56^{bright}CD16⁻ pbNK cells shared 73 DEGs with
304 non-adaptive trNK cells in lung, including high expression of *ITGAI* (CD49a), *ZNF683*
305 (Hobit), *PRDMI* (Blimp-1), *CCL5*, *PIK3R1*, *PLA2G16*, *ATXN1*, as well as lower
306 expression of *SELL* (CD62L), *GPR183*, *IL18R1*, *IL18RAP*, *SOX4*, *RAMP1*, and
307 *IFITM3* (Fig. 6B). All of these genes have also been shown to be differentially
308 expressed in trNK cells in the bone marrow and/or CD8⁺ T_{RM} cells in lung (32,34). It
309 should however be noted that other core-genes associated with tissue-resident
310 lymphocytes (e.g. *SIPRI*, *SIPR5*, *CXCR6*, *ITGAE*, *RGS1*, *KLF2*, *KLF3*, and *RIPOR2*)
311 were not differentially expressed between adaptive-like CD49a⁺CD56^{bright}CD16⁻ pbNK

312 cells and non-adaptive CD56^{bright}CD16⁻NK cells, indicating that they only partially
313 have a tissue-resident phenotype.

314 Next, we determined whether adaptive-like CD49a⁺CD56^{bright}CD16⁻ pbNK
315 share a common gene signature with adaptive-like trNK cells and/or CD56^{dim}CD16⁺
316 pbNK cells. Indeed, adaptive-like CD49a⁺CD56^{bright}CD16⁻ pbNK cells shared
317 differentially expressed genes with adaptive-like trNK cells in lung (Fig. 6C) and/or
318 CD56^{dim}CD16⁺ pbNK cells (8,25), including increased expression of *KIRs*, *KLRC2*,
319 *GZMH*, *ITGAD*, *CCL5*, *IL32*, *ZBTB38*, *CD3E*, *ARID5B*, *MCOLN2*, and *CD52*, and
320 decreased expression of *KLRB1*, *FCER1G*, *IL18RAP*, *IL2RB2*, *TLE1*, *AREG*, and
321 *KLRF1* (Fig. 6A, C, Supplementary Fig. 3).

322 Taken together, adaptive-like CD49a⁺CD56^{bright}CD16⁻ pbNK cells share traits with
323 both non-adaptive lung trNK cells, and adaptive-like trNK and CD56^{dim}CD16⁺ pbNK
324 cells.

325 Discussion

326 Human adaptive-like NK cells have been described within the CD56^{dim}CD16⁺
327 subset in peripheral blood (5,6,8,10,35) and the CD56^{bright}CD16⁻ subset in liver (7).
328 Here, we identified and characterized a yet unexplored and unique subset of adaptive-
329 like CD49a⁺KIR⁺NKG2C⁺CD56^{bright}CD16⁻ trNK cells in the human lung, paired blood,
330 and in unrelated healthy human blood. Lung adaptive-like trNK cells shared several
331 phenotypic features with other adaptive-like NK cell subsets both in blood and/or liver,
332 including high expression of CD49a (liver), CD69 (liver), CD2 (blood) and lack of, or
333 decreased expression of CD57 (liver), CD45RA (liver) and perforin (liver), as well as
334 low expression of FcεR1γ and Siglec-7 (blood) (5,7-10,21,35,36). However, lung
335 adaptive-like trNK cells segregate from liver adaptive-like trNK cells on the basis of
336 high expression of Eomes and CD103, and from adaptive-like CD56^{dim}CD16⁺ pbNK
337 cells by lack of CD57 and a CD56^{bright}CD16⁻ phenotype (7). Transcriptome analysis
338 revealed shared core genes in adaptive-like trNK cells, and CD56^{dim}CD16⁺ and
339 CD56^{bright}CD16⁻ pbNK cells, underlining common features between all adaptive-like
340 NK cell populations. Intriguingly, lung adaptive-like trNK cells were highly target cell-
341 responsive, and the overall paired blood and lung NK cell populations were
342 hyperresponsive in donors with expansions of adaptive-like trNK cells in the lung.
343 These findings indicate *in vivo* priming akin to what has been observed previously in
344 human antigen-dependent (3,37), antigen-independent, and cytokine-dependent (2,38-
345 40) NK cell recall responses. Furthermore, adaptive-like CD56^{dim}CD16⁺ pbNK cells
346 have recently been shown to be functionally primed against target cells following IL-
347 12 and IL-18 stimulation, while showing only a poor response to these cytokines alone
348 (41). In line with our results, this emphasizes a role of potential cytokine-mediated
349 priming of adaptive-like trNK cells in the human lung.

350 Despite the indications of *in vivo* priming, the presence of expansions of
351 adaptive-like CD49a⁺CD56^{bright}CD16⁻ NK cells in the lung donors did not correlate
352 with presence or kind of tumor, HCMV serostatus, or clinical and demographic
353 parameters. In fact, we could identify adaptive-like CD49a⁺CD56^{bright}CD16⁻ NK cells
354 also in the peripheral blood of healthy donors. These adaptive-like
355 CD49a⁺CD56^{bright}CD16⁻ pbNK cells shared a gene signature with trNK cells in the
356 human lung, indicating tissue imprinting. These findings suggest re-entry of adaptive-
357 like trNK cells from tissue into circulation and, hence, potential seeding of tissues with
358 adaptive-like trNK cells via peripheral blood. In mice, CD8⁺ T effector cells egress
359 from infected lung in a tightly regulated manner following infection with influenza A
360 virus (42), and CD8⁺ T_{RM} cells wane over time in self-limiting viral infections of the
361 respiratory tract (43). MCMV-specific CD8⁺ T cells convert to CD103⁺ T_{RM} cells, with
362 small numbers of new T_{RM} cells deriving from the circulation (44), and memory
363 inflation is required for retention of CD8⁺ T_{RM} cells in the lungs after intranasal
364 vaccination with MCMV (45). This indicates a dynamic retention of T_{RM} cells by a
365 persistent infection. It remains to be determined whether virus-dependent expansion
366 and maintenance of T_{RM} cells is analogous in adaptive-like trNK cells in the lung.
367 However, our data indicate that T_{RM} cells and adaptive-like NK cells differ at least in
368 their recruitment to the lung, with T_{RM} cells being dependent on CXCR6 (46) while
369 adaptive-like CD49a⁺CD56^{bright}CD16⁻ pbNK cells lacked CXCR6 but expressed high
370 levels of CXCR3.

371 Adaptive-like CD49a⁺CD56^{bright}CD16⁻ NK cell expansions were rarely
372 observed in donors with adaptive-like CD56^{dim}CD16⁺ pbNK cell expansions, indicating
373 that these two distinct subsets have different developmental cues. Indeed, even in the
374 rare cases where we could detect expansions of both adaptive-like
375 CD49a⁺CD56^{bright}CD16⁻ NK cells and CD56^{dim}CD16⁺ pbNK cells in the same

376 individual, these populations displayed specific and individual KIR repertoires.
377 Furthermore, expansions of adaptive-like lung trNK cells were detected in HCMV-
378 seronegative individuals (Supplementary Fig. 2E, F), while expansions of adaptive-like
379 CD56^{dim}CD16⁺ pbNK cells were restricted to HCMV-seropositive individuals
380 (Supplementary Fig. 2E) (5,35). It thus remains possible that other viral infections than
381 CMV in humans and mice (1,47,48) could drive the expansion of adaptive-like trNK
382 cells, as has previously been suggested for the generation of cytokine-induced memory
383 NK cells, e.g. after influenza virus infection in humans (49) and mice (4,50,51), as well
384 as vesicular stomatitis virus (VSV) (4), vaccinia virus (52), HIV-1 (4), and herpes
385 simplex virus 2 (HSV-2) (51), and after immunization with simian immunodeficiency
386 virus (SIV) in rhesus macaques (53). Taken together, our data support a model where
387 adaptive-like trNK cells and CD56^{dim}CD16⁺ pbNK cells develop independently from
388 each other, possibly due to distinct environmental requirements for their expansion.

389 We observed increased gene expression levels of *GZMH* in adaptive-like
390 CD49a⁺CD56^{bright}CD16⁻ lung and blood NK cells, and levels for *CCL5* were higher in
391 both conventional and adaptive-like lung trNK cells as compared to CD69⁻
392 CD56^{bright}CD16⁻ lung NK cells, and particularly highly expressed in adaptive-like
393 CD49a⁺CD56^{bright}CD16⁻ pbNK cells. An antiviral activity has been proposed for
394 granzyme H (54,55), however, a direct association of this effector molecule with
395 adaptive-like NK cells remains to be determined. In contrast, *CCL5* and *XCL1*, which
396 are both upregulated in human CD49a⁺CD56^{bright}CD16⁻ adaptive-like NK cells, were
397 predominantly produced by mouse Ly49H⁺ NK cells upon stimulation with MCMV-
398 derived m157 protein (56), and *CCL5* has been shown to be specifically expressed by
399 CD8⁺ memory T_{EM} cells (57). Thus, adaptive-like CD49a⁺CD56^{bright}CD16⁻ blood and
400 lung NK cells share functional characteristics with other memory lymphocyte
401 populations. Furthermore, we showed that adaptive-like lung trNK cells were

402 hyperresponsive against target cells, hence, they might be clinically relevant e.g. in
403 disease progression in respiratory viral infections and/or the defense against malignant
404 tumor cells. Similarly, lung CD8⁺ T_{RM} cells have previously been shown to be able to
405 control tumor growth and to correlate with increased survival in lung cancer patients
406 (58). Since adaptive-like trNK cells likely exceed their circulating pbNK cell
407 counterpart in tissue-homing and tumor-infiltration based on their expression of tissue-
408 specific receptors such as CD49a and CXCR3, these cells could be harnessed for future
409 treatment options of solid tumors.

410 Together, our data reveal the presence of a yet unexplored and distinct adaptive-
411 like trNK cell subset in the human lung, indicating that adaptive-like NK cells are not
412 confined to peripheral blood and/or liver and that different lineages of adaptive-like NK
413 cells potentially exist. Expansions of adaptive-like trNK cells in the lung were
414 commonly accompanied by the presence of adaptive-like CD49a⁺CD56^{bright}CD16⁻ NK
415 cells in paired peripheral blood, enabling the non-invasive identification of donors with
416 potential adaptive-like lung trNK cell expansions as well as the isolation of adaptive-
417 like NK cells with tissue-resident characteristics. Finally, adaptive-like NK cells with
418 tissue-resident features and excessive functional responsiveness in the human lung and
419 blood could be an attractive source for tailored cancer immunotherapies, in particular
420 for targeting solid tumors.

421 **Acknowledgements**

422 The authors acknowledge support from the National Genomics Infrastructure in
423 Stockholm funded by Science for Life Laboratory, the Knut and Alice Wallenberg
424 Foundation, the Swedish Research Council, and SNIC/Uppsala Multidisciplinary
425 Center for Advanced Computational Science for assistance with massively parallel
426 sequencing and access to the UPPMAX computational infrastructure. The authors also
427 acknowledge the MedH Core Flow Cytometry Facility (Karolinska Institutet),
428 supported by Karolinska Institutet and Region Stockholm, for providing cell-sorting
429 services. Furthermore, the authors want to thank all donors for participating in the study
430 and A.-C. Orre, V. Jackson, and S. Hylander for administrative and clinical help as well
431 as E. Yilmaz for assistance in the laboratory. **Funding:** This work was supported by
432 the Swedish Research Council, the Strategic Research Foundation, the Swedish
433 Foundation for Strategic Research, the Swedish Cancer Society, Sweden's Innovation
434 Agency, the Eva and Oscar Ahréns Research Foundation, Stockholm, the Åke Wiberg
435 Foundation and the Tornspiran Foundation.

436

437 **Author contribution:** Conceptualization: N.M., H.G.L., Ja.M.; Methodology: N.M.,
438 Ja.M.; Investigation: N.M., M.S., Je.M., J.H., E.K., M.B., S.N., J.N.W.; Resources:
439 M.A.-A.; Writing – original draft: N.M., Ja.M.; Writing – review and editing: N.M.,
440 Ja.M., H.G.L; Visualization: N.M., Ja.M.; Funding acquisition: N.M., Ja.M., H.G.L.

441

442 **Competing Interests:** The authors declare no competing financial interest.

443 **Figure legends**

444 **Figure 1: Adaptive-like KIR⁺NKG2C⁺ NK cells exist in the CD56^{bright}CD16⁻ NK**
445 **cell subset in the human lung. (A)** Representative overlay displaying pan-KIR and
446 NKG2C expression on CD56^{dim}CD16⁺ NK cells in paired blood (black contour) and
447 lung (orange). **(B)** Representative dot plots displaying pan-KIR and NKG2C expression
448 on CD56^{bright}CD16⁻ NK cells in the lungs of three different donors. **(C)** Summary of
449 data showing the frequencies of KIR⁺NKG2C⁺ NK cells in CD56^{dim}CD16⁺ and
450 CD56^{bright}CD16⁻ NK cells in paired blood and lung (n = 77). Friedman test, Dunn's
451 multiple comparisons test. ***p<0.001, ****p<0.0001. **(D)** UMAP analysis of
452 CD56^{bright}CD16⁻ lung NK cells from four donors with 2,000 events/donor (942 events
453 in one of the donors). UMAPs were constructed using expression of Siglec-7, CD8,
454 CD2, CD57, CD161, NKG2C, CD56, CD45RA, NKG2A and NKp80. Color scale
455 shows log₂(normalized expression + 1). **(E)** Representative histograms and **(F)**
456 summary of data showing surface expression of NKG2A (n = 27), CD57 (n = 27),
457 Siglec-7 (n = 7), CD161 (n = 12), CD2 (n = 5), ILT2 (n = 6), CD8 (n = 20), NKp80 (n
458 = 6), CD45RA (n = 5), and intracellular expression of FcεR1γ (n = 4), Eomes (n = 7)
459 and T-bet (n = 6) in KIR⁺NKG2C⁺ NK cells in CD56^{dim}CD16⁺ blood (grey) and lung
460 (orange) NK cells and CD56^{bright}CD16⁻ lung NK cells (blue). Friedman test, Dunn's
461 multiple comparisons test. *p<0.05, **p<0.01, ***p<0.001, ****p<0.0001.

462

463 **Figure 2: Adaptive-like CD56^{bright}CD16⁻ lung NK cells are tissue-resident. (A)**
464 Overlay of UMAPs from data from Figure 1, showing the position of NKG2C⁺ (blue)
465 and NKG2C⁻ (grey) populations among CD56^{bright}CD16⁻ NK cells. **(B)** Expression of
466 the tissue-residency markers CD69, CD49a, and CD103 within the UMAP of
467 CD56^{bright}CD16⁻ lung NK cells. **(C)** Representative histograms and **(D)** summary of
468 data showing the expression of the tissue-residency markers CD69 (n = 23), CD49a (n=

469 21) and CD103 (n = 21) on CD56^{dim}CD16⁺ blood (grey) and lung (orange) NK cells
470 and CD56^{bright}CD16⁻ lung NK cells (blue), respectively. Friedman test, Dunn's multiple
471 comparisons test. *p<0.05, **p<0.01, ***p<0.001, ****p<0.0001. **(E)** Heatmap
472 showing 102 differentially expressed genes between KIR⁺NKG2C⁺ trNK cells and
473 KIR⁻NKG2C⁻ trNK cells in the human lung. Differentially expressed genes shared with
474 CD57⁺NKG2C⁺CD56^{dim}CD16⁺ adaptive-like NK cells in blood (from GSE117614) are
475 highlighted in red. **(F)** Log2 fold-change for non-adaptive (NKG2C⁻) trNK cells vs
476 adaptive-like trNK cells in lung against log2 fold change for CD57⁺NKG2C⁻ vs
477 adaptive-like CD57⁺NKG2C⁺ CD56^{dim} NK cells in blood. Data for CD56^{dim} NK cells
478 in peripheral blood are from GSE117614 (25). **(G-I)** Single KIR expression analysis on
479 CD56^{dim}CD16⁺ NK cells from peripheral blood (red), CD49a⁻CD103⁻CD56^{dim}CD16⁺
480 or CD103⁻CD56^{dim}CD16⁺ (black) and CD49a⁺CD103⁺CD56^{bright}CD16⁻ or
481 CD103⁺CD56^{bright}CD16⁻ (blue) NK cells in matched lung of three different donors.
482 Educating KIR are highlighted in red. **(G)** Donor with expansions of self-KIR⁺ NK cells
483 both in the CD56^{dim}CD16⁺ subset in paired blood and lung and in the CD56^{bright}CD16⁻
484 NK cell subset in the lung. **(H)** Donor with an expansion of self-KIR⁺ NK cells
485 exclusively in the CD56^{bright}CD16⁻ NK cell subset in the lung. **(I)** Donor with
486 expansions of self-KIR⁺ NK cells both in the CD56^{dim}CD16⁺ and CD56^{bright}CD16⁻
487 subsets in paired blood and lung, respectively.

488

489 **Figure 3: Adaptive-like lung trNK cells are highly functional.** **(A)** Gene expression
490 levels (counts per million reads) for selected genes associated with functional capacity
491 are shown for non-adaptive CD49a⁺KIR⁻NKG2C⁻ and adaptive-like
492 CD49a⁺KIR⁺NKG2C⁺ lung trNK cells (clear circles: CD49a⁺CD103⁻ NK cells, filled
493 circles: CD49a⁺CD103⁺ NK cells). Mean ± SEM is shown. **(B)** Representative
494 histograms and **(C)** summary of data displaying expression of perforin and granzyme

495 B (GzmB) (n = 4) in CD56^{dim}CD16⁺ and in non-adaptive CD49a⁻CD56^{bright}CD16⁻ as
496 well as adaptive-like CD49a⁺CD56^{bright}CD16⁻ NK cells, respectively, in human lung *ex*
497 *vivo*. CD14⁻CD19⁻CD3⁻CD45⁺CD127⁺CD161⁺ cells were gated as controls in (B).
498 Friedman test, Dunn's multiple comparisons test. *p<0.05. **(D)** Representative dot plots
499 showing expression of CD107a and CD49a on KIR⁻NKG2C⁻ and KIR⁺NKG2C⁺ NK
500 cells in a donor without (upper panel) and with (lower panel) expansion of adaptive-
501 like trNK cells in the lung (expression KIR and NKG2C are displayed in the left panel
502 for each of the two donors). **(E)** Summary of data showing the frequency of K562 target
503 cell-induced CD107a⁺ (left) and TNF⁺ (right) NK cell subsets from donors with NK
504 cell expansions in the human lung. Responses by unstimulated controls were subtracted
505 from stimulated cells (n = 4). Mean ± SD is shown. **(F)** Representative dot plots
506 showing expression of CD107a and TNF vs CD103 on non-adaptive CD49a⁺KIR⁻
507 NKG2C⁻ (upper panel) or adaptive-like CD49a⁺KIR⁺NKG2C⁺ (lower panel) bulk NK
508 cells in a donor with an expansion of adaptive-like trNK cells in the lung. **(G, H)**
509 Summary of data showing the frequencies of **(G)** CD107a⁺ and **(H)** TNF⁺ NK cells in
510 blood NK cells and in subsets of lung NK cells (CD49a⁻CD103⁻, expressing either
511 CD49a or CD103, or CD49a⁺CD103⁺) from donors without (left panels, n = 5 for
512 CD107a, n= for TNF) or with (right panels, n = 5) expansions of KIR⁺NKG2C⁺ trNK
513 cells in the lung. Responses by unstimulated controls were subtracted from stimulated
514 cells. (G, H) Violin plots with quartiles and median are shown. Friedman test, Dunn's
515 multiple comparisons test. *p<0.05.

516

517 **Figure 4: Expansions of adaptive-like trNK cell in the lung indicate presence of**
518 **adaptive-like CD49a⁺CD56^{bright}CD16⁻ NK cells in paired blood.** **(A)** Representative
519 dot plots displaying expression of CD49a and NKG2C on NK cells in lung and paired
520 peripheral blood. **(B)** Summary of data of frequencies of adaptive-like CD49a⁺ NK cells

521 of CD16⁻ trNK cells and of adaptive-like pbNK cells in the CD16⁺ NK cell subset in
522 paired lung and peripheral blood. Adaptive-like NK cell “expansions” were identified
523 as outliers (filled circles) using the Robust regression and Outlier removal (ROUT)
524 method (ROUT coefficient Q=1). Error bars show the median with interquartile range
525 (n = 86). Median with interquartile range is shown. **(C)** Euler diagram indicating
526 overlaps and relationships between adaptive-like trNK and pbNK cell expansions in
527 peripheral blood and lung. The number of individuals with overlaps between the subsets
528 and compartments are indicated in the circles. **(D)** Representative overlays and **(E)**
529 summary of data showing phenotypic differences between adaptive-like CD49a⁺ (blue)
530 and non-adaptive CD49a⁻ (grey) NK cells within the CD56^{bright}CD16⁻ NK cell subset
531 in blood. (NKG2A, n=6; CD57, n=5; CD69, n=6; CD103, n=6; CD127, n=3; CD161,
532 n=4). Violin plots with quartiles and median are shown.

533

534 **Figure 5: Expansions of adaptive-like CD49a⁺CD56^{bright}CD16⁻ NK cells in healthy**
535 **blood donors. (A)** Representative dot plot (left plot) and overlay (right plot) showing
536 expression of KIR and NKG2C (left plot), and CD49a on adaptive-like KIR⁺NKG2C⁺
537 NK cells (blue) versus non-adaptive KIR⁻NKG2C⁻ NK cells (grey) (right plot) within
538 CD16⁻ blood NK cells of healthy blood donors. **(B)** Identification of expansions (filled
539 circles) of adaptive-like CD56^{dim}CD16⁺ pbNK cells (21 outliers, 20%) and adaptive-
540 like CD49a⁺CD56^{bright}CD16⁻ pbNK cells (17 outliers, 16%) via the ROUT method (see
541 also Figure 4E). Error bars show the median with interquartile range. (n=95). Median
542 with interquartile range is shown. **(C)** Frequencies of KIR⁺NKG2C⁺ cells of CD49a⁻
543 CD16⁻ or CD49a⁺CD16⁻ NK cells in healthy blood. The respective maternal population
544 comprised at least 45 cells (n=13). Wilcoxon matched-pairs signed rank test. **p<0.005
545 **(D)** UMAPs based on CD56^{bright}CD16⁻ NK cells from three donors with
546 KIR⁺NKG2C⁺CD56^{bright}CD16⁻ NK cells. UMAPs were constructed using expression

547 of CXCR3, CD161, Ki67, NKG2C, CD103, TIGIT, perforin, granzyme B, NKG2A,
548 CD16, CD56, CD49a, CD38, CD8, CXCR6, CD4, CD57, CD45RA, NKp80, CD69,
549 GL183/EB6 (KIR), and CD127. Color scale indicates $\log_2(\text{normalized protein}$
550 $\text{expression} + 1)$ for each parameter. **(E)** Summary of protein expression on adaptive-like
551 CD49a^+ NK cells from peripheral blood from healthy donors. (CD69, n=11; CD103,
552 n=7; CD57, n=11; NKG2A, n=11; CD127, n=7; CD161, n=7; CD8, n=11; CD38, n=5;
553 CD45RA, n=4; NKp80, n=5; TIM-3, n=5; CXCR3, n=4; CXCR6, n=5; Ki67, n=5;
554 perforin, n=7; granzyme B, n=5). Violin plots with quartiles and median are shown. **(F)**
555 Gene expression levels (counts per million reads) for selected genes associated with
556 functional capacity are shown for $\text{CD49a}^-\text{KIR}^-$ and $\text{CD49a}^+\text{KIR}^+$ blood
557 $\text{CD56}^{\text{bright}}\text{CD16}^-$ NK cells. Mean \pm SEM is shown.

558

559 **Figure 6: Adaptive-like $\text{CD49a}^+\text{CD56}^{\text{bright}}\text{CD16}^-$ pbNK cells in healthy blood**
560 **donors share traits with both trNK cells and with adaptive-like trNK cells. (A)**
561 Heatmap showing 138 differentially expressed genes ($\text{padj} < 0.001$, $\log_2\text{FC} > 2$) between
562 adaptive-like $\text{CD49a}^+\text{CD56}^{\text{bright}}\text{CD16}^-$ NK cells and non-adaptive CD49a^-
563 $\text{CD56}^{\text{bright}}\text{CD16}^-$ NK cells in peripheral blood from unrelated healthy donors (n=4).
564 Genes shared with trNK cells in the lung were highlighted in dark blue, shared with
565 adaptive-like trNK cells in bright blue, and genes shared with adaptive-like
566 $\text{CD56}^{\text{dim}}\text{CD16}^+$ pbNK cells in orange. **(B)** Log₂ fold-change for trNK cells vs non-
567 tissue-resident $\text{CD56}^{\text{bright}}\text{CD16}^-$ NK cells in lung against log₂ fold-change for adaptive-
568 like $\text{CD49a}^+\text{CD56}^{\text{bright}}\text{CD16}^-$ vs non-adaptive $\text{CD49a}^-\text{CD56}^{\text{bright}}\text{CD16}^-$ NK cells in
569 blood. **(C)** Log₂ fold-change for $\text{KIR}^+\text{NKG2C}^+$ trNK cells vs NKG2C^- trNK cells in
570 lung against log₂ fold-change for adaptive-like $\text{CD49a}^+\text{CD56}^{\text{bright}}\text{CD16}^-$ vs non-
571 adaptive $\text{CD49a}^-\text{CD56}^{\text{bright}}\text{CD16}^-$ NK cells in blood.

572

573 Table 1. Clinical and demographic details of the 103 patients included in the study.

574

	Never-smoker (n = 16)	Current smoker (n = 25)	Ex-smoker (n = 62)
Female / male	8 / 8	14 / 11	41 / 21
Age (y), mean ± SD	67 ± 13.4	67 ± 8.0	69 ± 7.1
FEV1/FVC (% of predicted) mean ± SD	100 ± 10.3	88 ± 13.7*	93 ± 14.9 [#]
Pathology	% (n)	% (n)	% (n)
Non-malignant	6 (1)	4 (1)	2 (1)
Adenocarcinoma	44 (7)	52 (13)	76 (47)
Large cell carcinoma	0 (0)	12 (3)	3 (2)
Squamous cell carcinoma	6 (1)	16 (4)	5 (3)
Metastasis	0 (0)	4 (1)	3 (2)
Carcinoid	31 (5)	8 (2)	6 (4)
Adenosquamous carcinoma	6 (1)	0 (0)	3 (2)
Other [§]	6 (1)	4 (1)	2 (1)
Medication	% (n)	% (n)	% (n)
Inhaled corticosteroids	19 (3)	0 (0)	2 (1)
Statins	38 (6)	28 (7)	31 (19)
Systemic immunosuppression	0 (0)	4 (1)	5 (3)
Beta-agonists or anti-cholinergics	0 (0)	12 (3)	13 (8)
Inhaled corticosteroid and long-acting beta-agonist combination	0 (0)	8 (2)	6 (4)
Diagnoses affecting lung function	% (n)	% (n)	% (n)
Asthma	19 (3)	0 (0)	5 (3)
COPD	0 (0)	32 (8)	10 (6)
Other lung parenchyme disease	6 (1)	0 (0)	2 (1)

575 * n = 24

576 # n = 59

577 § = uncertain histopathological diagnosis, data missing, combined small cell carcinoma

578

579 **Material and methods**

580 *Lung patients and healthy blood*

581 A total of 103 patients undergoing lobectomy for suspected lung cancer were included
582 in this study for collection of lung tissue and paired peripheral blood. None of the
583 patients received preoperative chemotherapy and/or radiotherapy. Patients with records
584 of strong immunosuppressive medication and/or hematological malignancy were
585 excluded from the study. Clinical and demographic details are summarized in Table 1.
586 Furthermore, healthy blood was collected from regular, unrelated blood donors. The
587 regional review board in Stockholm approved the study, and all donors gave informed
588 written consent prior to collection of samples.

589

590 *Processing of tissue specimens and peripheral blood*

591 Lung tissue was processed as previously described (18). Briefly, a small part of
592 macroscopically tumor-free human lung tissue from each patient was transferred into
593 ice-cold Krebs-Henseleit buffer and stored on ice for less than 18 h until further
594 processing. The tissue was digested using collagenase II (0.25 mg/ml, Sigma-Aldrich)
595 and DNase (0.2 mg/ml, Roche), filtered and washed in complete RPMI 1640 medium
596 (Thermo Scientific) supplemented with 10% FCS (Thermo Scientific), 1 mM L-
597 glutamine (Invitrogen), 100 U/ml penicillin, and 50 µg/ml streptomycin (R10 medium).
598 Finally, mononuclear cells from the lung cell suspensions and peripheral blood were
599 isolated by density gradient centrifugation (Lymphoprep).

600

601 *RNA-sequencing and RNAseq data analysis*

602 RNA of sorted NK cell subsets from blood and lung were sequenced and analyzed as
603 described previously (15). Briefly, RNAseq was performed using a modified version of
604 the SMART-Seq2 protocol (59). For analysis of lung adaptive-like NK cells, live

605 NKG2C⁺KIR⁺CD3⁻CD14⁻CD19⁻CD56⁺CD16⁻ NK cells were sorted from two donors
606 and were compared to previously published data on CD69⁺CD49a⁺CD103⁻ and
607 CD69⁺CD49a⁺CD103⁺ NKG2A⁺CD16⁻ trNK cells (GSE130379) (15). For analysis of
608 KIR⁺CD49a⁺ CD56^{bright}CD16⁻ NK cells, we sorted KIR⁺CD49a⁺ and KIR⁻CD49a⁻ live
609 CD14⁻CD19⁻CD3⁻CD56^{bright}CD16⁻ NK cells from cryopreserved PBMCs from 4
610 donors. Duplicates of 100 cells from each population from two individual donors were
611 sorted into 4.2ul of lysis buffer (0.2% Triton X-100, 2.5uM oligo-dT (5'-
612 AAGCAGTGGTATCAACGCAGAGTACT30VN-3'), 2.5mM dNTP, RNase
613 Inhibitor (Takara), and ERCC RNA spike in controls (Ambion)) in a 96-well V-bottom
614 PCR plate (Thermo Fisher). Sorted cells were then frozen and stored at -80°C until they
615 could be processed. Subsequent steps were performed following the standard SMART-
616 Seq2 protocol with 22 cycles of cDNA amplification and sample quality was
617 determined using a bioanalyzer (Agilent, High Sensitivity DNA chip). 5ng of amplified
618 cDNA was taken for tagmentation using a customized in-house protocol (60) and
619 Nextera XT primers. Pooled samples were sequenced on a HiSeq2500 on high output
620 mode with paired 2x125bp reads.

621

622 *Transcriptome analysis*

623 Following sequencing and demultiplexing, read pairs were trimmed from Illumina
624 adapters using cutadapt (version 1.14) (61), and UrQt was used to trim all bases with a
625 phred quality score below 20 (62). Read pairs were subsequently aligned to the protein
626 coding sequences of the human transcriptome (gencode.v26.pc_transcripts.fa) using
627 Salmon (version 0.8.2) (63), and gene annotation using gencode.v26.annotation.gtf.
628 DeSeq2 (64) was used to analyze RNA-seq data in R studio version 1.20. Briefly, raw
629 count values were used as input into deSeq2, and variance stabilizing transformation
630 was used to transform data. Data were batch- and patient corrected using Limma (65).

631 A cut-off of >100 counts across the samples was used to filter out low expressed genes.
632 Genes with an adjusted p-value<0.05 and a log2-fold change greater than 1 were
633 considered as differentially expressed between paired samples. Similarly, previously
634 published data sets on adaptive-like NKG2C⁺CD57⁺CD56^{dim}CD16⁺ NK cells and
635 conventional NKG2C⁻CD57⁺CD56^{dim} NK cells (GSE117614) (25) were analyzed using
636 deSeq2 to identify differentially expressed genes. Heatmaps of gene expression were
637 generated using Pheatmap in R and show the z-score for differentially expressed genes
638 (as determined above in deSeq2) for all donors and replicates.

639

640 *Flow cytometry*

641 Antibodies and clones reactive against the following proteins were used: CD2 (TS1/8,
642 BV421 or Pacific Blue, Biolegend), CD3 (UCHT1, PE-Cy5, Beckman Coulter), CD8
643 (RPA-T8, Brilliant Violet 570, Biolegend, or RPA-8, BUV395 or SK1, BUV737, BD
644 Biosciences), CD14 (MφP9, Horizon V500, BD Biosciences), CD16 (3G8, Brilliant
645 Violet 570 or Brilliant Violet 711, or Brilliant Violet 785, Biolegend), CD19 (HIB19,
646 Horizon V500, BD Biosciences), CD38 (HIT2, Brilliant Violet 711 or BUV661, BD
647 Biosciences), CD45 (HI30, Alexa Fluor 700, Biolegend, or BUV805, BD Biosciences),
648 CD45RA (HI100, Brilliant Violet 785, Biolegend), CD49a (TS2A, AlexaFluor 647,
649 Biolegend, or HI30, BUV615, or 8R84, Brilliant Violet 421, BD Biosciences), CD56
650 (N901, ECD, Beckman Coulter, or HCD56, Brilliant Violet 711, Biolegend, or
651 NCAM16.2, PE-Cy7, or BUV563, BD Biosciences), CD57 (TB01, purified,
652 eBioscience, or HNK-1, Brilliant Violet 605, Biolegend), CD103 (APC, B-Ly7,
653 eBioscience, or biotin, 2G5, Beckman Coulter, or Ber-ACT8, Brilliant Violet 711,
654 BUV395, BD Biosciences, or Ber-ACT8, PE-Cy-7, Biolegend), KIR2DL1
655 (FAB1844F, biotin, R&D Systems), KIR2DL3 (180701, FITC, R&D Systems),
656 KIR3DL1 (DX9, Brilliant Violet 421, Biolegend), KIR3DL2 (DX-31, Brilliant Violet

657 711, Biolegend), KIR2DL2/S2/L3 (GL183, PE-Cy5.5, Beckman Coulter),
658 KIR2DL1/S1 (EB6, PE-Cy5.5 or PE-Cy7, Beckman Coulter), NKG2A (Z1991.10,
659 APC-A780, or PE, Beckman Coulter, or 131411, BUV395, BD Biosciences), NKG2C
660 (134591, Alexa-Fluor 488 or PE, R&D Systems), CD69 (TP1.55.3, ECD, Beckman
661 Coulter, or FN50, PE-CF594, BD Biosciences, or FN50, Brilliant Violet 786,
662 Biolegend), CD127 (Brilliant Violet 421, HIL-7R-M21, BD Biosciences or PE-Cy7,
663 R34.34, Beckman Coulter), CD161 (HP3-3G10, Brilliant Violet 605 or APC/Fire 750,
664 Biolegend), CXCR3 (Alexa Fluor 647, G025H7, Biolegend), CXCR6 (K041E5,
665 Brilliant Violet 421, Biolegend), CD85j/ILT2 (HP-F1, Super Bright 436, Invitrogen),
666 NKp80 (5D12, PE, BD Biosciences, or 4A4.D10, PE-Vio770, Miltenyi), Siglec-7 (5-
667 386, Alexa Fluor 488, Bio-Rad), TIM-3 (7D3, Brilliant Violet 711, BD Biosciences).
668 After two washes, cells were stained with streptavidin Qdot 605 or Qdot 585 (both
669 Invitrogen), anti-mouse IgM (II/41, eFluor 650NC, eBioscience) and Live/Dead Aqua
670 (Invitrogen). After surface staining, peripheral blood mononuclear cells (PBMC) were
671 fixed and permeabilized using FoxP3/Transcription Factor staining kit (eBioscience).
672 For intracellular staining the following antibodies were used: Eomes (WF1928, FITC,
673 eBioscience), Fc ϵ R1 γ (polyclonal, FITC, Merck), granzyme B (GB11, BB790, BD
674 Biosciences), Ki67 (B56, Alexa Fluor 700, BD Biosciences), perforin (dG9, BB755,
675 BD Biosciences, or B-D48, Brilliant Violet 421, Biolegend), T-bet (4B10, Brilliant
676 Violet 421, BD Biosciences), and TNF (MAb11, Brilliant Violet 421, Biolegend, or
677 Brilliant Violet 650, BD Biosciences). Purified NKG2C (134591, R&D Systems) was
678 biotinylated using a Fluoreporter Mini-biotin XX protein labeling kit (Life
679 Technologies) and detected using streptavidin-Qdot 585, 605 or 655 (Invitrogen).
680 Samples were analyzed on a BD LSR Fortessa equipped with four lasers (BD
681 Biosciences) or a BD FACSymphony A5 equipped with five lasers (BD Biosciences),
682 and data were analyzed using FlowJo version 9.5.2 and version 10.6.1 (Tree Star Inc).

683 UMAPs were constructed in FlowJo 10.6.1 using the UMAP plugin. UMAP
684 coordinates and protein expression data were subsequently exported from FlowJo, and
685 protein expression for each parameter was normalized to a value between 0 and 100.
686 UMAP plots were made in R using ggplot, and color scale show log₂(normalized
687 protein expression +1).

688 For sorting of NK cells from lung and peripheral blood for RNA sequencing,
689 thawed cryopreserved mononuclear cells were stained with anti-human CD57 (NK-1,
690 FITC, BD Biosciences), CD16 (3G2, Pacific Blue, BD Biosciences), CD14 (MφP9,
691 Horizon V500, BD Biosciences), CD19 (HIB19, Horizon V500, BD Biosciences),
692 CD103 (Ber-ACT8, Brilliant Violet 711, BD Biosciences), CD49a (TS2/7, Alexa Fluor
693 647, Biolegend), CD45 (HI30, A700, Biolegend), CD8 (RPA-T8, APC/Cy7, BD
694 Biosciences), NKG2A (Z199.10, PE, Beckman Coulter), CD69 (TP1.55.3, ECD,
695 Beckman Coulter), CD3 (UCHT1, PE/Cy5, Beckman Coulter), KIR2DL1/S1 (EB6,
696 PE/Cy5.5, Beckman Coulter), KIR2DL2/3/S2 (GL183, PE/Cy5.5, Beckman Coulter),
697 NKG2C (134591, biotin, R&D Systems, custom conjugate), CD56 (NCAM16.1,
698 PE/Cy7, BD Biosciences), streptavidin Qdot655 (Invitrogen), and Live/Dead Aqua
699 (Invitrogen).

700

701 *DNA isolation and KIR/HLA-ligand genotyping*

702 Genomic DNA was isolated using a DNeasy Blood & Tissue Kit (Qiagen) from 100 µl
703 of whole blood. KIR genotyping and KIR ligand-determination were performed using
704 PCR-SSP technology with a *KIR* typing kit and a *KIR HLA* ligand kit (both Olerup-
705 SSP) according to the manufacturer's instructions.

706

707 *CMV IgG ELISA*

708 Concentrations of anti-CMV IgG relative to a standard curve and internal negative and
709 positive control were determined by ELISA (Abcam, UK) and read in a microplate
710 spectrophotometer (Bio-Rad xMark) at 450nm with a 620nm reference wavelength.

711

712 *Activation assay*

713 Degranulation and TNF production of fresh blood and lung NK cells were assessed as
714 previously described (18,19). In brief, fresh lung and blood mononuclear cells were
715 resuspended in R10 medium and rested for 15 to 18 hours at 37°C. Subsequently, the
716 cells were co-cultured in R10 medium alone or in presence of K562 cells for 2 hours in
717 the presence of anti-human CD107a (FITC or Brilliant Violet 421, H4A3, BD
718 Biosciences, San Jose, Calif.).

719

720 *Statistics*

721 GraphPad Prism 6 and 7 (GraphPad Software) was used for statistical analysis.
722 For each analysis, measurements were taken from distinct samples. The statistical
723 method used is indicated in each figure legend.

724

725 **Data Availability**

726 The dataset generated for this study can be found in the Gene Expression Omnibus with
727 accession no. **xxxxx** (data will be deposited and made available before publication).

728 **References**

729

730

731 1. Sun JC, Beilke JN, Lanier LL. Adaptive immune features of natural killer cells. *Nature*.
732 2009 Jan 29;457(7229):557–61.

733 2. Cooper MA, Elliott JM, Keyel PA, Yang L, Carrero JA, Yokoyama WM. Cytokine-
734 induced memory-like natural killer cells. *Proceedings of the National Academy of*
735 *Sciences of the United States of America*. 2009 Feb 10;106(6):1915–9.

736 3. O'Leary JG, Goodarzi M, Drayton DL, Andrian von UH. T cell- and B cell-independent
737 adaptive immunity mediated by natural killer cells. *Nature immunology*. 2006
738 May;7(5):507–16.

739 4. Paust S, Gill HS, Wang B-Z, Flynn MP, Moseman EA, Senman B, et al. Critical role for
740 the chemokine receptor CXCR6 in NK cell-mediated antigen-specific memory of
741 haptens and viruses. *Nature immunology*. 2010 Dec;11(12):1127–35.

742 5. Guma M, Angulo A, Vilches C, Gomez-Lozano N, Malats N, Lopez-Botet M. Imprint of
743 human cytomegalovirus infection on the NK cell receptor repertoire. *Blood*. 2004 ed.
744 2004 Dec 1;104(12):3664–71.

745 6. Lopez-Vergès S, Milush J, Schwartz B, Pando M, Jarjoura J, York V, et al. Expansion
746 of a unique CD57⁺NKG2Chi natural killer cell subset during acute human
747 cytomegalovirus infection. *Proceedings of the National Academy of Sciences of the*
748 *United States of America*. 2011;108(36):14725–32.

749 7. Marquardt N, Béziat V, Nyström S, Hengst J, Ivarsson MA, Kekäläinen E, et al. Cutting
750 Edge: Identification and Characterization of Human Intrahepatic CD49a⁺ NK Cells. *J*
751 *Immunol*. 2015 Feb 11;194(6):2467–71.

752 8. Schlums H, Cichocki F, Tesi B, Theorell J, Béziat V, Holmes TD, et al.
753 Cytomegalovirus infection drives adaptive epigenetic diversification of NK cells with
754 altered signaling and effector function. *Immunity*. 2015 Mar 17;42(3):443–56.

755 9. Lee J, Zhang T, Hwang I, Kim A, Nitschke L, Kim M, et al. Epigenetic modification and
756 antibody-dependent expansion of memory-like NK cells in human cytomegalovirus-
757 infected individuals. *Immunity*. 2015 Mar 17;42(3):431–42.

758 10. Béziat V, Liu LL, Malmberg J-A, Ivarsson MA, Sohlberg E, Björklund AT, et al. NK cell
759 responses to cytomegalovirus infection lead to stable imprints in the human KIR
760 repertoire and involve activating KIRs. *Blood*. 2013 Apr 4;121(14):2678–88.

761 11. Cerwenka A, Lanier LL. Natural killer cell memory in infection, inflammation and
762 cancer. *Nature reviews Immunology*. 2016 Feb;16(2):112–23.

763 12. Kuijpers TW, Baars PA, Dantin C, van den Burg M, van Lier RAW, Roosnek E. Human
764 NK cells can control CMV infection in the absence of T cells. *Blood*. 2008 Aug
765 1;112(3):914–5.

766 13. Chen Z, Yang Y, Liu LL, Lundqvist A. Strategies to Augment Natural Killer (NK) Cell
767 Activity against Solid Tumors. *Cancers (Basel)*. Multidisciplinary Digital Publishing
768 Institute; 2019 Jul 23;11(7):1040.

769 14. Menaes E, Gálvez-Cancino F, Cáceres-Morgado P, Ghorani E, López E, Díaz X, et
770 al. Tissue-resident memory CD8⁺ T cells amplify anti-tumor immunity by triggering
771 antigen spreading through dendritic cells. *Nat Commun*. Nature Publishing Group;
772 2019 Sep 27;10(1):4401–12.

- 773 15. Marquardt N, Kekäläinen E, Chen P, Lourda M, Wilson JN, Scharenberg M, et al.
774 Unique transcriptional and protein-expression signature in human lung tissue-resident
775 NK cells. *Nat Commun. Nature Publishing Group*; 2019 Aug 26;10(1):3841–12.
- 776 16. Cooper GE, Ostridge K, Khakoo SI, Wilkinson TMA, Staples KJ. Human CD49a+ Lung
777 Natural Killer Cell Cytotoxicity in Response to Influenza A Virus. *Front Immunol.*
778 *Frontiers*; 2018;9:1671.
- 779 17. Gordon CL, Miron M, Thome JJC, Matsuoka N, Weiner J, Rak MA, et al. Tissue
780 reservoirs of antiviral T cell immunity in persistent human CMV infection. *The Journal*
781 *of experimental medicine*. 2017 Mar 6;214(3):651–67.
- 782 18. Marquardt N, Kekäläinen E, Chen P, Kvedaraite E, Wilson JN, Ivarsson MA, et al.
783 Human Lung NK Cells are Predominantly Comprised of Highly Differentiated
784 Hypofunctional CD69(-)CD56(dim) Cells. *J Allergy Clin Immunol*. 2016 Sep
785 23;139(4):1321–4.
- 786 19. Scharenberg M, Vangeti S, Kekäläinen E, Bergman P, Al-Ameri M, Johansson N, et
787 al. Influenza A Virus Infection Induces Hyperresponsiveness in Human Lung Tissue-
788 Resident and Peripheral Blood NK Cells. *Front Immunol. Frontiers*; 2019;10:1116.
- 789 20. Chiesa Della M, Falco M, Podestà M, Locatelli F, Moretta L, Frassoni F, et al.
790 Phenotypic and functional heterogeneity of human NK cells developing after umbilical
791 cord blood transplantation: a role for human cytomegalovirus? *Blood*. 2012 Jan
792 12;119(2):399–410.
- 793 21. Liu LL, Landskron J, Ask EH, Enqvist M, Sohlberg E, Traherne JA, et al. Critical Role
794 of CD2 Co-stimulation in Adaptive Natural Killer Cell Responses Revealed in NKG2C-
795 Deficient Humans. *Cell Rep*. 2016 May 3;15(5):1088–99.
- 796 22. Emgård J, Kammoun H, García-Cassani B, Chesné J, Parigi SM, Jacob J-M, et al.
797 Oxysterol Sensing through the Receptor GPR183 Promotes the Lymphoid-Tissue-
798 Inducing Function of Innate Lymphoid Cells and Colonic Inflammation. *Immunity*. 2018
799 Jan 16;48(1):120–8.
- 800 23. Adams NM, Lau CM, Fan X, Rapp M, Geary CD, Weizman O-E, et al. Transcription
801 Factor IRF8 Orchestrates the Adaptive Natural Killer Cell Response. *Immunity*. 2018
802 Jun 19;48(6):1172–6.
- 803 24. Lau CM, Adams NM, Geary CD, Weizman O-E, Rapp M, Pritykin Y, et al. Epigenetic
804 control of innate and adaptive immune memory. *Nature immunology. Nature*
805 *Publishing Group*; 2018 Sep;19(9):963–72.
- 806 25. Cichocki F, Wu C-Y, Zhang B, Felices M, Tesi B, Tuininga K, et al. ARID5B regulates
807 metabolic programming in human adaptive NK cells. *The Journal of experimental*
808 *medicine. Rockefeller University Press*; 2018 Sep 3;215(9):2379–95.
- 809 26. Foley B, Cooley S, Verneris MR, Pitt M, Curtsinger J, Luo X, et al. Cytomegalovirus
810 reactivation after allogeneic transplantation promotes a lasting increase in educated
811 NKG2C+ natural killer cells with potent function. *Blood*. 2012 Mar 15;119(11):2665–
812 74.
- 813 27. Kim S-H, Han S-Y, Azam T, Yoon D-Y, Dinarello CA. Interleukin-32: a cytokine and
814 inducer of TNFalpha. *Immunity*. 2005 Jan;22(1):131–42.
- 815 28. Ray SJ, Franki SN, Pierce RH, Dimitrova S, Kotliansky V, Sprague AG, et al. The
816 collagen binding alpha1beta1 integrin VLA-1 regulates CD8 T cell-mediated immune
817 protection against heterologous influenza infection. *Immunity*. 2004 Feb;20(2):167–79.

- 818 29. Cheuk S, Schlums H, Gallais S  r  zal I, Martini E, Chiang SC, Marquardt N, et al.
819 CD49a Expression Defines Tissue-Resident CD8(+) T Cells Poised for Cytotoxic
820 Function in Human Skin. *Immunity*. 2017 Feb 21;46(2):287–300.
- 821 30. Vento-Tormo R, Efremova M, Botting RA, Turco MY, Vento-Tormo M, Meyer KB, et al.
822 Single-cell reconstruction of the early maternal-fetal interface in humans. *Nature*.
823 Nature Publishing Group; 2018 Nov;563(7731):347–53.
- 824 31. Masopust D, Choo D, Vezys V, Wherry EJ, Duraiswamy J, Akondy R, et al. Dynamic T
825 cell migration program provides resident memory within intestinal epithelium. *The*
826 *Journal of experimental medicine*. 2010 Mar 15;207(3):553–64.
- 827 32. Kumar BV, Ma W, Miron M, Granot T, Guyer RS, Carpenter DJ, et al. Human Tissue-
828 Resident Memory T Cells Are Defined by Core Transcriptional and Functional
829 Signatures in Lymphoid and Mucosal Sites. *Cell Rep*. 2017 Sep 19;20(12):2921–34.
- 830 33. Sojka DK, Plougastel-Douglas B, Yang L, Pak-Wittel MA, Artyomov MN, Ivanova Y, et
831 al. Tissue-resident natural killer (NK) cells are cell lineages distinct from thymic and
832 conventional splenic NK cells. *Elife*. 2014;3:e01659.
- 833 34. Melsen JE, Lugthart G, Vervat C, Kielbasa SM, van der Zeeuw SAJ, Buermans HPJ,
834 et al. Human Bone Marrow-Resident Natural Killer Cells Have a Unique
835 Transcriptional Profile and Resemble Resident Memory CD8+ T Cells. *Front Immunol*.
836 *Frontiers*; 2018;9:1829.
- 837 35. B  ziat V, Dalgard O, Asselah T, Halfon P, Bedossa P, Boudifa A, et al. CMV drives
838 clonal expansion of NKG2C+ NK cells expressing self-specific KIRs in chronic
839 hepatitis patients. *Eur J Immunol*. 2012;42(2):447–57.
- 840 36. Hammer Q, R  ckert T, Romagnani C. Natural killer cell specificity for viral infections.
841 *Nature immunology*. Nature Publishing Group; 2018 Aug;19(8):800–8.
- 842 37. Nikzad R, Angelo LS, Aviles-Padilla K, Le DT, Singh VK, Bimler L, et al. Human
843 natural killer cells mediate adaptive immunity to viral antigens. *Sci Immunol*. *Science*
844 *Immunology*; 2019 May 10;4(35):eaat8116.
- 845 38. Romee R, Schneider SE, Leong JW, Chase JM, Keppel CR, Sullivan RP, et al.
846 Cytokine activation induces human memory-like NK cells. *Blood*. 2012 Dec
847 6;120(24):4751–60.
- 848 39. Romee R, Rosario M, Berrien-Elliott MM, Wagner JA, Jewell BA, Schappe T, et al.
849 Cytokine-induced memory-like natural killer cells exhibit enhanced responses against
850 myeloid leukemia. *Sci Transl Med*. American Association for the Advancement of
851 *Science*; 2016 Sep 21;8(357):357ra123–3.
- 852 40. Ni J, H  lsken O, Miller M, Hammer Q, Luetke-Eversloh M, Romagnani C, et al.
853 Adoptively transferred natural killer cells maintain long-term antitumor activity by
854 epigenetic imprinting and CD4+ T cell help. *Oncoimmunology*. Taylor & Francis;
855 2016;5(9):e1219009.
- 856 41. Hammer Q, R  ckert T, Dunst J, Romagnani C. Adaptive Natural Killer Cells Integrate
857 Interleukin-18 during Target-Cell Encounter. *Front Immunol*. *Frontiers*; 2017;8:1976.
- 858 42. Jennrich S, Lee MH, Lynn RC, Dewberry K, Debes GF. Tissue exit: a novel control
859 point in the accumulation of antigen-specific CD8 T cells in the influenza A virus-
860 infected lung. *Journal of virology*. 2012 Apr;86(7):3436–45.
- 861 43. Wu T, Hu Y, Lee Y-T, Bouchard KR, Benechet A, Khanna K, et al. Lung-resident
862 memory CD8 T cells (TRM) are indispensable for optimal cross-protection against
863 pulmonary virus infection. *J Leukoc Biol*. Wiley-Blackwell; 2014 Feb;95(2):215–24.

- 864 44. Smith CJ, Caldeira-Dantas S, Turula H, Snyder CM. Murine CMV Infection Induces
865 the Continuous Production of Mucosal Resident T Cells. *Cell Rep.* 2015 Nov
866 10;13(6):1137–48.
- 867 45. Morabito KM, Ruckwardt TJ, Bar-Haim E, Nair D, Moin SM, Redwood AJ, et al.
868 Memory Inflation Drives Tissue-Resident Memory CD8+ T Cell Maintenance in the
869 Lung After Intranasal Vaccination With Murine Cytomegalovirus. *Front Immunol.*
870 *Frontiers*; 2018;9:1861.
- 871 46. Takamura S, Kato S, Motozono C, Shimaoka T, Ueha S, Matsuo K, et al. Interstitial-
872 resident memory CD8+ T cells sustain frontline epithelial memory in the lung. *The*
873 *Journal of experimental medicine.* Rockefeller University Press; 2019 Sep
874 26;159:jem.20190557.
- 875 47. Orr M, Murphy W, Lanier L. “Unlicensed” natural killer cells dominate the response to
876 cytomegalovirus infection. *Nature immunology.* 2010;11(4):321–7.
- 877 48. Smith HRC, Heusel JW, Mehta IK, Kim S, Dorner BG, Naidenko OV, et al. Recognition
878 of a virus-encoded ligand by a natural killer cell activation receptor. *Proceedings of the*
879 *National Academy of Sciences of the United States of America.* 2002 Jun
880 25;99(13):8826–31.
- 881 49. Goodier MR, Rodríguez-Galán A, Lusa C, Nielsen CM, Darboe A, Moldoveanu AL, et
882 al. Influenza Vaccination Generates Cytokine-Induced Memory-like NK Cells: Impact
883 of Human Cytomegalovirus Infection. *J Immunol.* 2016 May 27.
- 884 50. Li T, Wang J, Wang Y, Chen Y, Wei H, Sun R, et al. Respiratory Influenza Virus
885 Infection Induces Memory-like Liver NK Cells in Mice. *J Immunol.* American
886 Association of Immunologists; 2017 Jan 23;198(3):1242–52.
- 887 51. Dou Y, Fu B, Sun R, Li W, Hu W, Tian Z, et al. Influenza vaccine induces intracellular
888 immune memory of human NK cells. *PLoS ONE.* 2015;10(3):e0121258.
- 889 52. Gillard GO, Bivas-Benita M, Hovav A-H, Grandpre LE, Panas MW, Seaman MS, et al.
890 Thy1+ NK [corrected] cells from vaccinia virus-primed mice confer protection against
891 vaccinia virus challenge in the absence of adaptive lymphocytes. *PLoS Pathog.* 2011
892 Aug;7(8):e1002141.
- 893 53. Reeves RK, Li H, Jost S, Blass E, Li H, Schafer JL, et al. Antigen-specific NK cell
894 memory in rhesus macaques. *Nature immunology.* 2015 Sep;16(9):927–32.
- 895 54. Tang H, Li C, Wang L, Zhang H, Fan Z. Granzyme H of cytotoxic lymphocytes is
896 required for clearance of the hepatitis B virus through cleavage of the hepatitis B virus
897 X protein. *J Immunol.* American Association of Immunologists; 2012 Jan
898 15;188(2):824–31.
- 899 55. Andrade F, Fellows E, Jenne DE, Rosen A, Young CSH. Granzyme H destroys the
900 function of critical adenoviral proteins required for viral DNA replication and granzyme
901 B inhibition. *EMBO J.* 2007 Apr 18;26(8):2148–57.
- 902 56. Dorner BG, Smith HRC, French AR, Kim S, Poursine-Laurent J, Beckman DL, et al.
903 Coordinate expression of cytokines and chemokines by NK cells during murine
904 cytomegalovirus infection. *J Immunol.* 2004 Mar 1;172(5):3119–31.
- 905 57. Swanson BJ, Murakami M, Mitchell TC, Kappler J, Marrack P. RANTES production by
906 memory phenotype T cells is controlled by a posttranscriptional, TCR-dependent
907 process. *Immunity.* 2002 Nov;17(5):605–15.

- 908 58. Nizard M, Roussel H, Diniz MO, Karaki S, Tran T, Voron T, et al. Induction of resident
909 memory T cells enhances the efficacy of cancer vaccine. *Nat Commun. Nature*
910 *Publishing Group*; 2017 May 24;8:15221.
- 911 59. Picelli S, Faridani OR, Björklund ÅK, Winberg G, Sagasser S, Sandberg R. Full-length
912 RNA-seq from single cells using Smart-seq2. *Nat Protoc. Nature Publishing Group*;
913 2014 Jan;9(1):171–81.
- 914 60. Picelli S, Björklund ÅK, Reinius B, Sagasser S, Winberg G, Sandberg R. Tn5
915 transposase and tagmentation procedures for massively scaled sequencing projects.
916 *Genome Res.* 2014 Dec;24(12):2033–40.
- 917 61. Martin M. Cutadapt removes adapter sequences from high-throughput sequencing
918 reads. *EMBnetjournal.* 2011 Aug 2;17(1):10.
- 919 62. Modolo L, Lerat E. UrQt: an efficient software for the Unsupervised Quality trimming of
920 NGS data. *BMC Bioinformatics.* 2015 Apr 29;16(1):175.
- 921 63. Patro R, Duggal G, Love MI, Irizarry RA, Kingsford C. Salmon provides fast and bias-
922 aware quantification of transcript expression. *Nature Methods.* 2017 Mar 6;14(4):417–
923 9.
- 924 64. Love MI, Huber W, Anders S. Moderated estimation of fold change and dispersion for
925 RNA-seq data with DESeq2. *Genome Biol. BioMed Central*; 2014;15(12):550.
- 926 65. Weigt SS, Wang X, Palchevskiy V, Gregson AL, Patel N, DerHovanessian A, et al.
927 Gene Expression Profiling of Bronchoalveolar Lavage Cells Preceding a Clinical
928 Diagnosis of Chronic Lung Allograft Dysfunction. *PLoS ONE. Public Library of*
929 *Science*; 2017;12(1):e0169894.
- 930

Figure 1

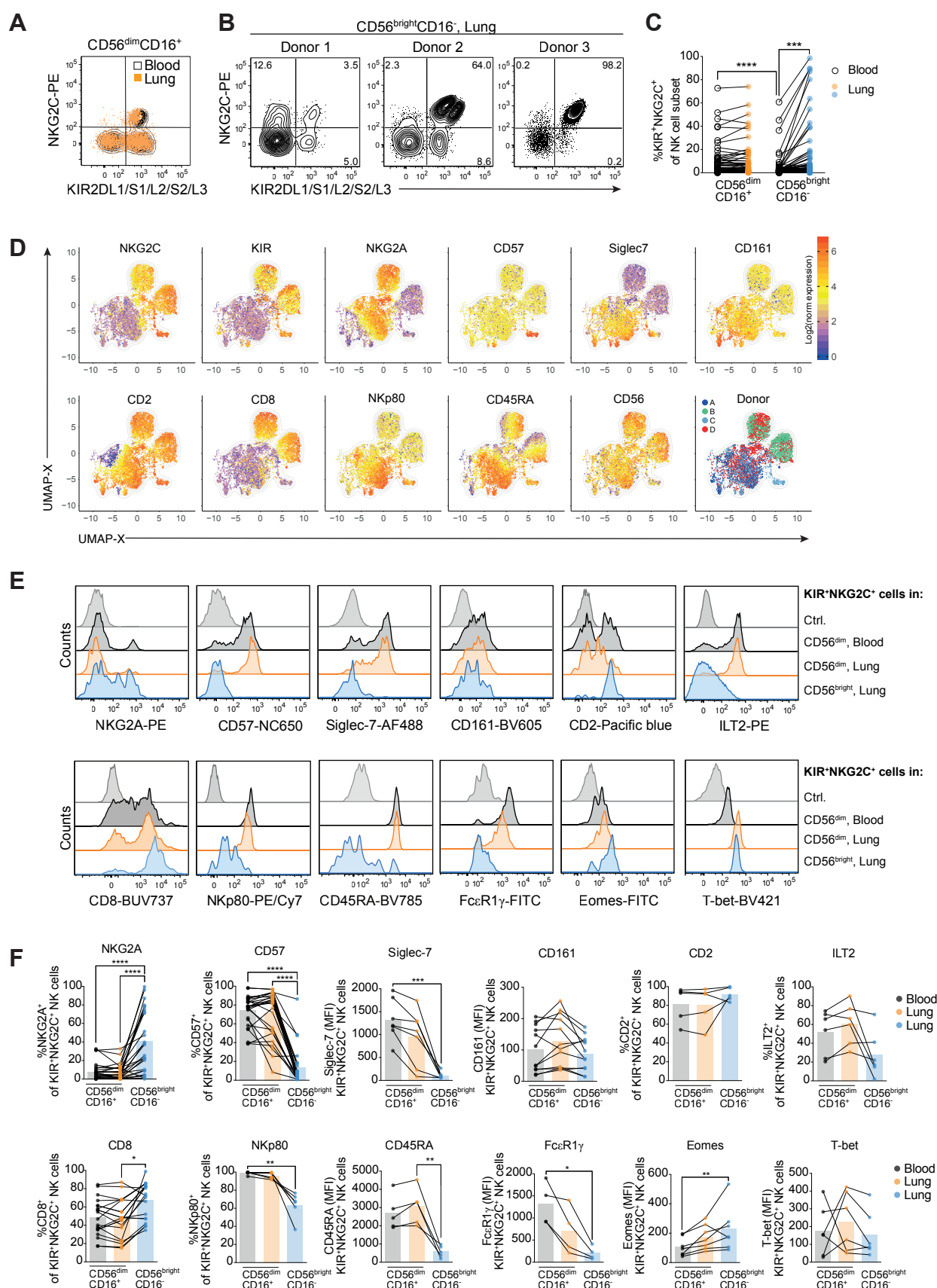


Figure 2

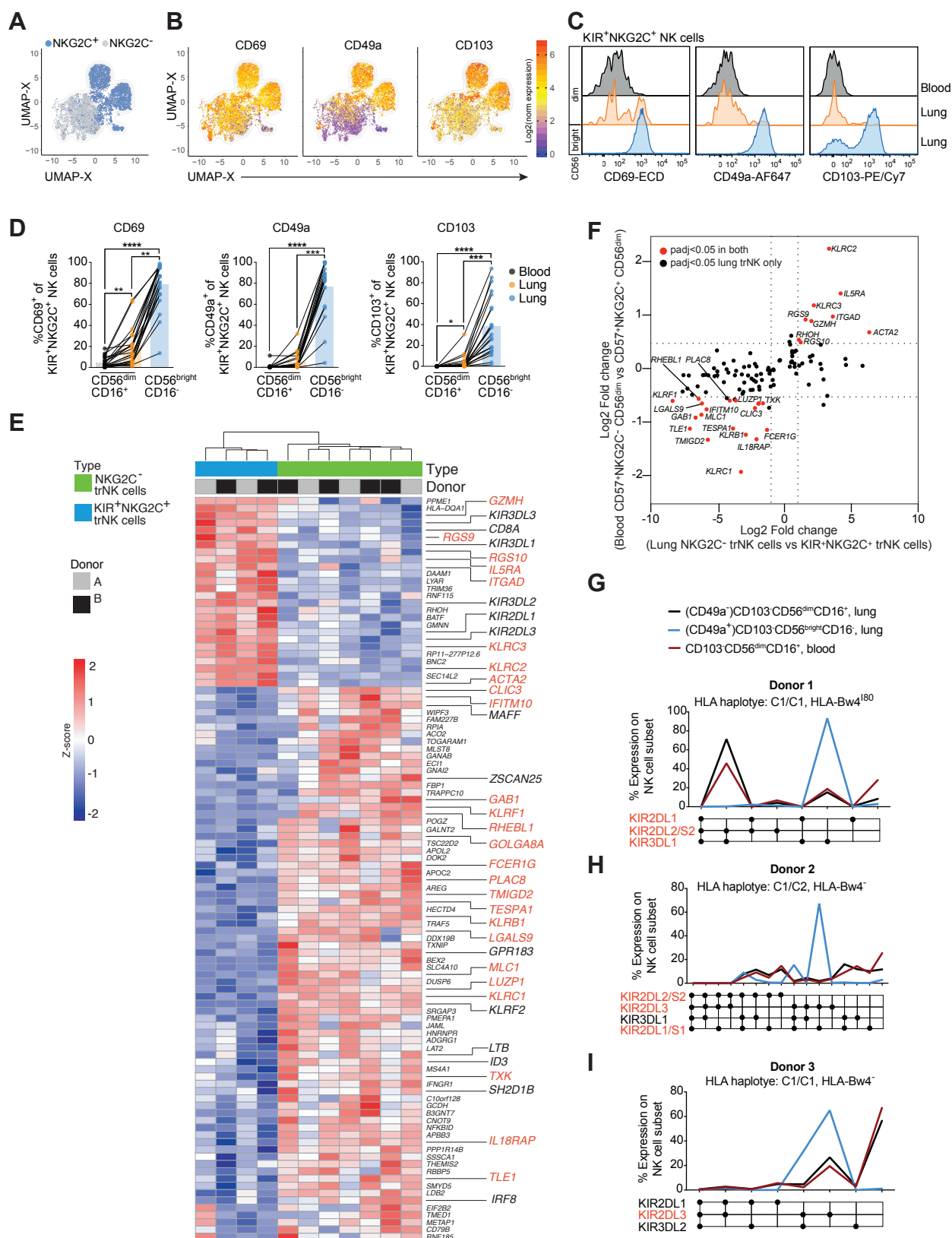


Figure 3

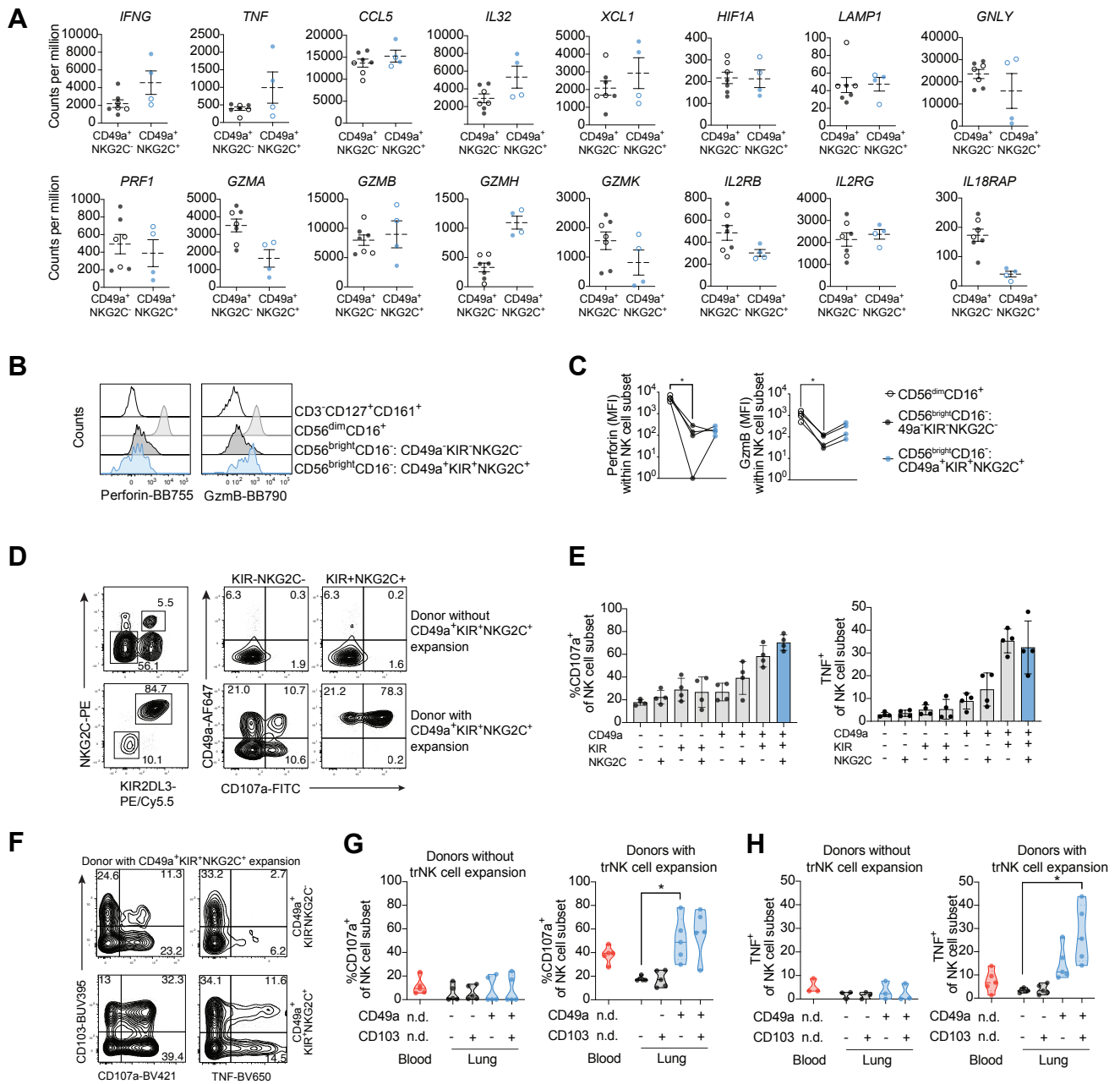


Figure 4

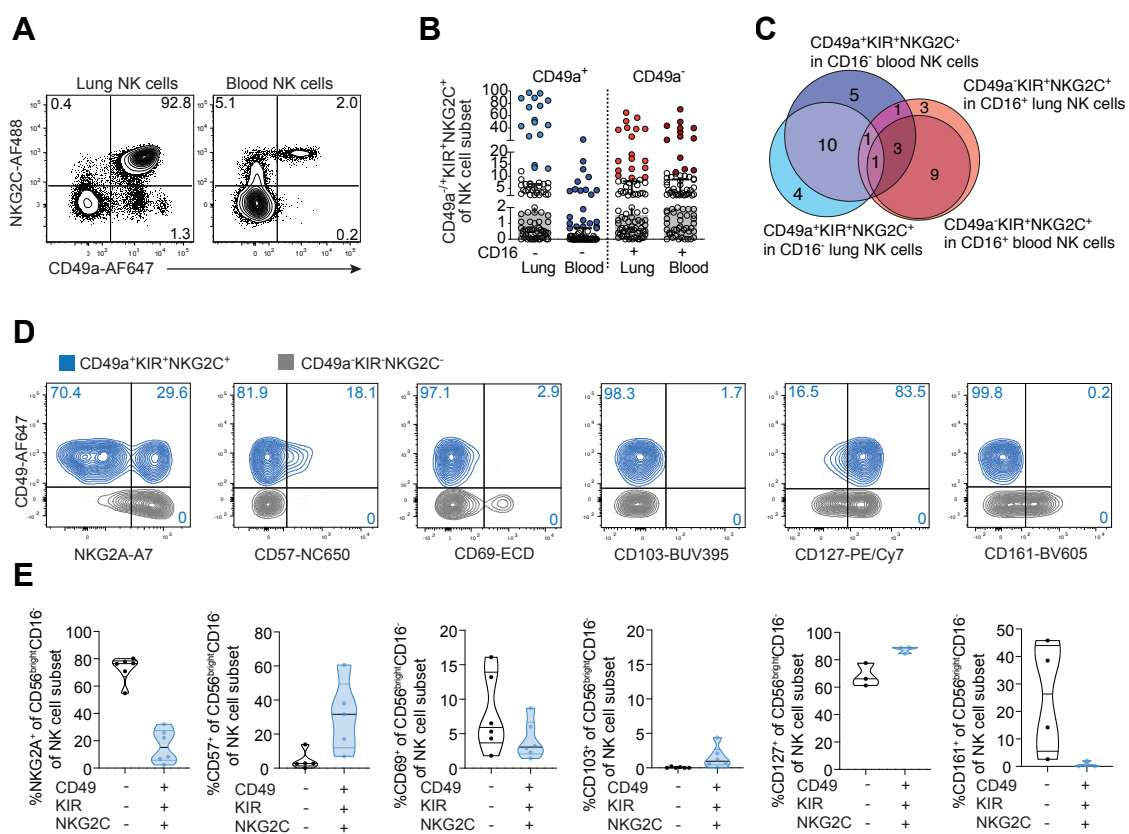


Figure 5

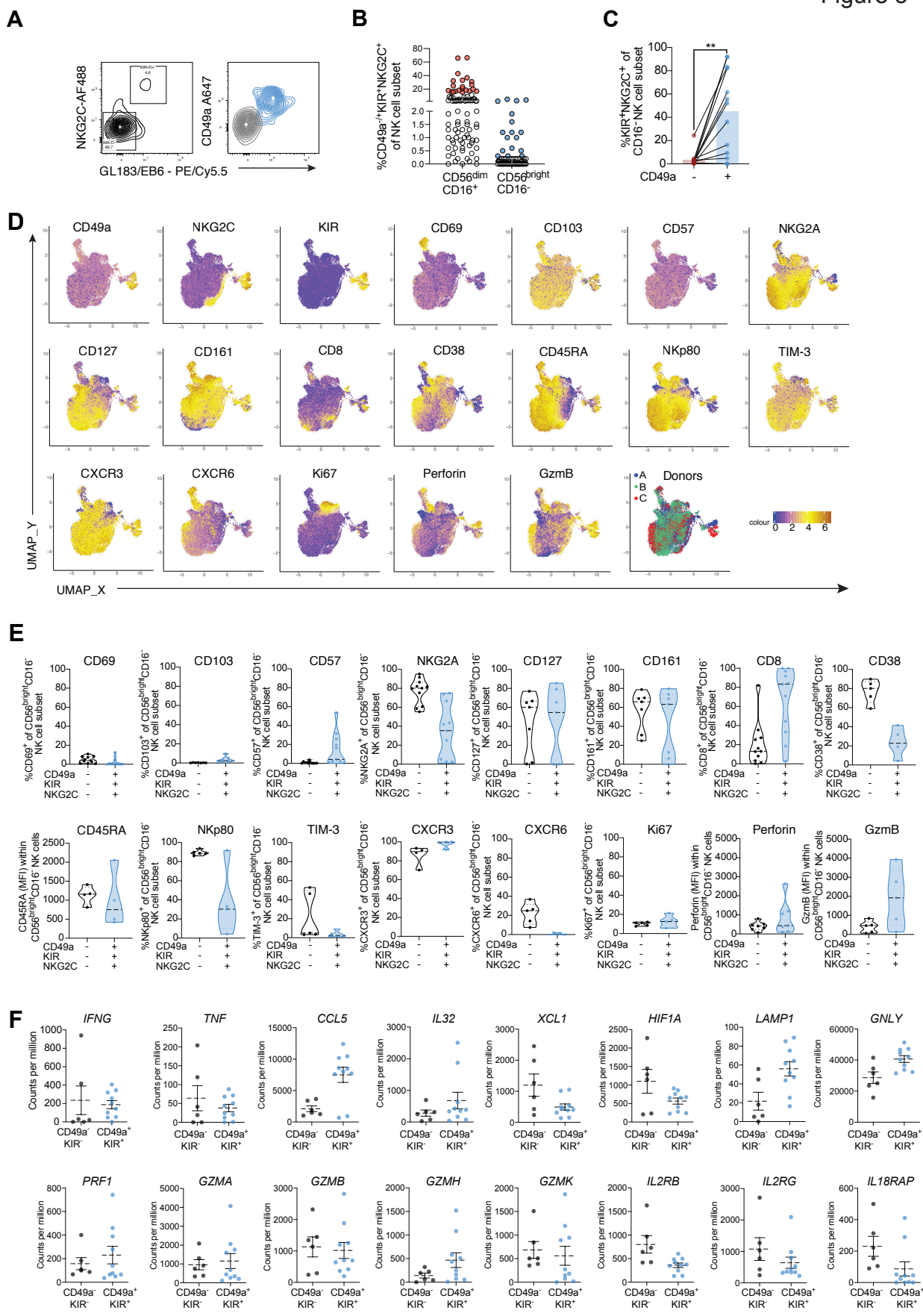


Figure 6

